Applied Geochemistry 151 (2023) 105597

Contents lists available at ScienceDirect

Applied Geochemistry

journal homepage: www.elsevier.com/locate/apgeochem

Simulating the source waters for the Wilkins Peak Member evaporite sequence with modern soda spring analogues

William D. Arnuk [a,*], Tim K. Lowenstein [a], Elizabeth M. Klonowski [a], Alan R. Carroll [b], M. Elliot Smith [c]

[a] Department of Geological Sciences, Binghamton University, State University of New York, United States
[b] Department of Geology and Geophysics, University of Wisconsin, United States
[c] Northern Arizona University, United States

ARTICLE INFO

Editorial handling by: Pablo Pasten

ABSTRACT

Chemical sediments of the lacustrine Wilkins Peak Member of the Eocene Green River Formation potentially preserve detailed paleoclimate information relating to the conditions of their formation and preservation within the lake basin during the Early Eocene Climatic Optimum. The Green River Formation comprises the world's largest sodium-carbonate evaporite deposit in the form of trona ($Na_2CO_3{\cdot}NaHCO_3{\cdot}2H_2O$) in the Bridger Basin and nahcolite ($NaHCO_3$) in the neighboring Piceance Creek Basin. Modern analogues suggest that these minerals necessitate the existence of an alkaline source water. Detrital provenance geochronometers suggest that the most likely source for volcanic waters to the Greater Green River Basin is the Colorado Mineral Belt, connected to the basin via the Aspen paleoriver.

Here, we test the hypothesis that magmatic waters from the Colorado Mineral Belt could have supplied the Greater Green River Basin with the alkalinity needed to precipitate sodium-carbonate evaporites that are preserved in the Wilkins Peak Member by numerically simulating the evaporation of modern soda spring waters from northwestern Colorado at various temperature and atmospheric pCO_2 conditions. The resulting simulated evaporite sequence is then compared to the mineralogy and textures preserved within the Wilkins Peak Member. Simulated evaporation of Steamboat Springs and Mineral Spring waters produce a close match to core observations and mineralogy. These simulations provide constraints on the salinities at which various minerals precipitated in the Wilkins Peak Member as well as insights into the regional temperature (>15 °C for gaylussite and trona; >27° for pirssonite and trona) and pCO_2 conditions (<1200 ppm for gaylussite and trona) during the Early Eocene Climatic Optimum.

1. Introduction

The Wilkins Peak Member (WPM) of the Eocene Green River Formation in the Greater Green River Basin (GGRB), Wyoming (Fig. 1), comprises a continuous 1.7-million-year (51.6–49.8 Ma) record of closed-basin lacustrine deposition (Smith et al., 2008a; Smith et al., 2003; Machlus et al., 2015; Smith et al., 2015; Jagniecki and Lowenstein, 2015). The WPM is known for its repetitive successions of calcitic and dolomitic mudstone, organic-rich "oil shale" mudstone, and its characteristic saline evaporites (Bradley, 1964). The sodium carbonate-bearing evaporites of the WPM, namely trona ($Na_2CO_3{\cdot}NaHCO_3{\cdot}2H_2O$) and nahcolite ($NaHCO_3$), plus halite (NaCl), form at specific ranges of temperature and pCO_2 (Lowenstein and Demicco, 2006; Jagniecki et al., 2013; Jagniecki and Lowenstein, 2015; Demicco and Lowenstein, 2020). Therefore, the evaporite sequences preserve important information regarding the climate and lake conditions at the time of deposition.

Regional paleoclimate conditions and potential sources of inflow water and solutes to the GGRB during the Early Eocene have been hypothesized (Lowenstein et al., 2017; Hammond et al., 2019). WPM sodium-carbonate evaporite deposits can provide a new test on whether or not various source waters can account for the inflow of alkalinity and solutes into the GGRB during the Early Eocene. Understanding the sources of alkalinity for the evaporite deposits of the lower WPM is

* Corresponding author. Department of Geological Sciences, Binghamton University, 4400 Vestal Parkway E, Science 1 Building, Binghamton, NY, 13902, United States.
E-mail address: warnuk1@binghamton.edu (W.D. Arnuk).

https://doi.org/10.1016/j.apgeochem.2023.105597
Received 24 August 2022; Received in revised form 3 January 2023; Accepted 10 February 2023
Available online 14 February 2023

integral to unraveling the paleohydrology of this ancient lake system, accurately interpreting the environmental and geologic conditions it records, and soda ash deposits in general.

The 642 m-long Solvay S-34-1 core, drilled in 2016 by Solvay Minerals in the depocenter of the Bridger Basin, contains a 250 m section of the WPM. The characteristic lithofacies observed in the Solvay core (Fig. 2) include carbonate mudstone, displacive evaporites in mudstone, bedded cumulate evaporites, and bottom-growth evaporites (Klonowski et al., 2022); these facies can serve as modeling targets for simulating the regional climatic and chemical conditions that led to their precipitation. Model simulations utilizing thermochemical data and the Pitzer ion-interaction model (Pitzer, 1991) can estimate the precipitation of Na-bearing evaporite minerals as a function of temperature, CO_2 concentration, and inflow water chemistry. Given the temperature and pCO_2 sensitivity of sodium carbonate-bearing minerals in the lower WPM of the Green River Formation, computer-simulated reconstructions of the evaporite record offer constraints on the temperature and pCO_2 conditions during the early Eocene (Lowenstein and Demicco, 2006; Demicco and Lowenstein, 2020; Olson and Lowenstein, 2021).

The sodium-carbonate evaporites, lithofacies, and plant fossils of the WPM suggest closed basin conditions, warm regional climate, and elevated atmospheric CO_2 (Wilf, 2000; Lowenstein and Demicco, 2006; Jagniecki et al., 2015; Demicco and Lowenstein, 2020). This study attempts to better constrain the potential sources of alkalinity necessary to precipitate the lower WPM evaporite sequences. We use modern soda spring waters from the Colorado Mineral Belt (CMB) and vicinity as a genetic analogue for ancient springs discharging from the same bedrock. Such alkaline spring inflow may have contributed to the solute load of the early Eocene Aspen paleoriver, which flowed from northwest Colorado into the GGRB (Hammond et al., 2019). We test whether evaporation of these soda spring waters can accurately produce the observed Green River mineral sequences.

2. Background

2.1. Green River Basin evaporite deposits

The GGRB is one of many Laramide intermontane basins in the Western USA, formed in response to basement deformation of the foreland of the North American Cordillera (e.g., Dickinson et al., 1988; Smith et al., 2015). Deposition of the WPM occurred during an underfilled phase of the GGRB (c.f. Carroll and Bohacs, 1999; Bohacs et al., 2000), and approximately coincided with the Early Eocene Climatic Optimum (EECO) (52.6–50.3 Ma) (Zachos et al., 2001, 2008). The WPM comprises repetitive successions of mud-cracked calcitic and dolomitic mudstone, organic-rich mudstone (oil shale), and evaporite, that together record expansion and contraction of paleolake Gosiute (Smoot, 1983; Pietras and Carroll, 2006; Smith et al., 2015). Carbonate-rich lacustrine facies are punctuated by arkosic fluvial deposits at ~100 Ky intervals (Culbertson, 1961; Aswasereelert et al., 2013; Smith et al., 2014). Evaporite facies are generally associated with sedimentologic evidence for perennial lakes (Jagniecki and Lowenstein, 2015), and include both bedded and displacive deposits. The former are especially prevalent within the lower WPM (Wiig et al., 1995; Smith et al., 2008a).

As lake brines become concentrated through evaporation, they precipitate a series of salts, controlled by the activities of the ionic reactants and the solubilities of the various precipitated saline minerals. The evolutive pathway of any particular brine is controlled by the limiting reactants involved in salt precipitation, which leads to chemical divides between different brine types (Hardie and Eugster, 1970; Drever, 1982). Chemical divides explain the formation of three major brine chemistries:

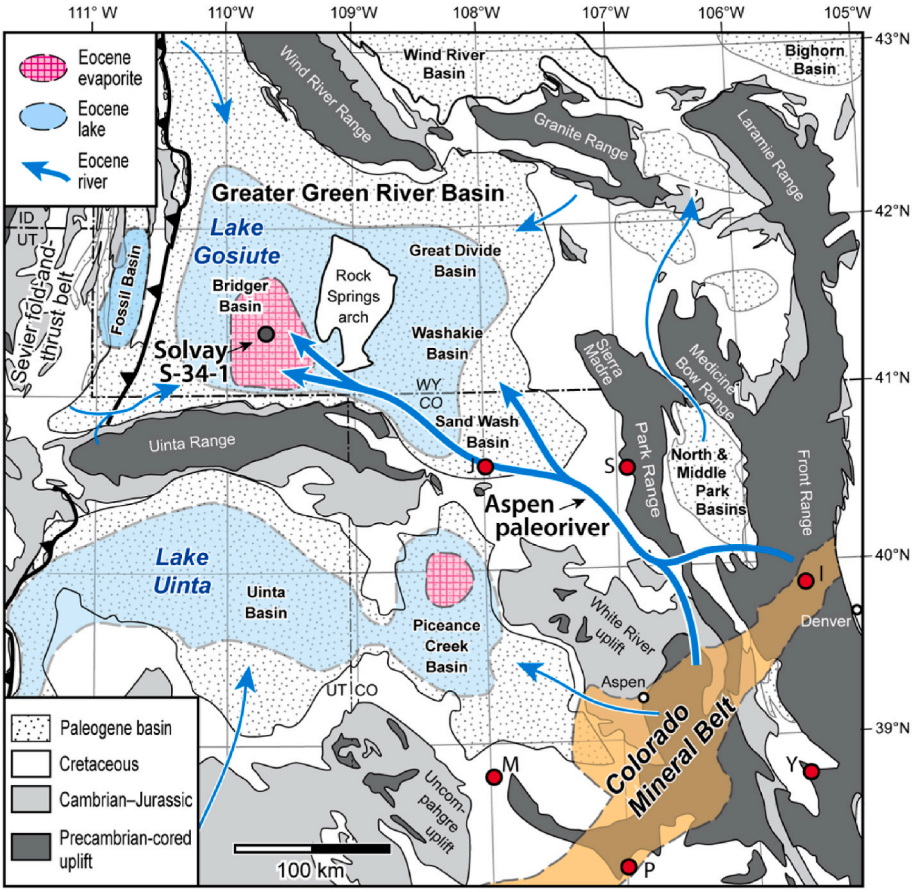

Fig. 1. Map of the Greater Green River Basin (Bridger Basin, Great Divide Basin, Washakie Basin, and Sand Wash Basin) and surrounding area showing the proposed inflow pathways of various Eocene Rivers, including the Aspen paleoriver from the Colorado Mineral Belt (modified from Hammond et al., 2019). Eocene lakes that filled the sub-basins in which the Green River Formation was deposited are shown in blue. The Colorado Mineral Belt is shown in orange and the locations of modern soda springs are highlighted in red. J = Juniper Spring; S = Steamboat Springs; I = Idaho Springs; M = Mineral Spring; P = Powder Horn Hot Spring; Y = Yellow Soda Spring.

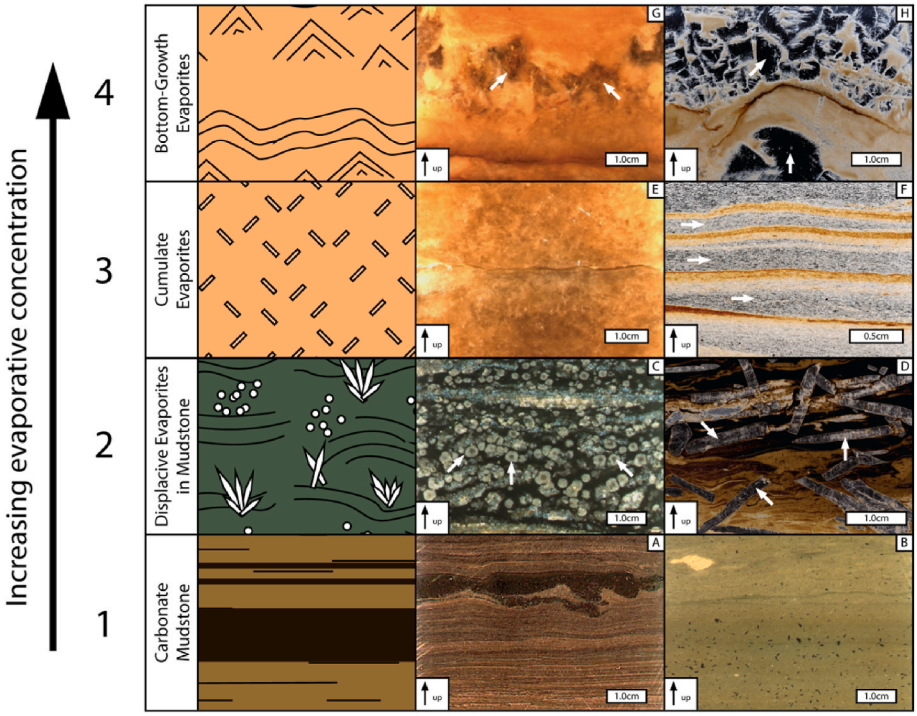

Fig. 2. Left column shows characteristic facies of the lower Wilkins Peak Member in the basin-center Solvay S-34-1 drill core (Klonowski et al., 2022). Center and right columns (boxes A-H) show examples of characteristic WPM facies from core slab photos and thin section photomicrographs of WPM cores. A: Solvay S-34-1 core photo, 640.3 m; B: Solvay S-34-1 core photo, 633.2 m; C: Solvay S-34-1 core photo, 578.6 m; D: Solvay S-34-1 core photomicrograph, 594.7 m; E: Solvay S-34-1 core photo, 621.1 m; F: ERDA Blacks Fork 1 core photomicrograph, 349.9 m; G: Solvay S-34-1 core photo, 560.1 m depth; H: Diamond Alkali Grierson 1 core photomicrograph, 539.8 m.

The least saline lithology (row 1), shown at bottom, is bedded carbonate mudstone, of predominantly dolomitic composition (B), and kerogen-rich "oil shale" (A), characterized by mm-scale laminations composed of lighter, carbonate-rich mudstone and darker mudstone rich in organic matter. Row 2 is carbonate mudstone with displacive evaporites (northupite (C) and shortite (D)). Shortite is interpreted as a high temperature replacement of gaylussite or pirssonite (Jagniecki et al., 2013). Large displacive crystals (D, shown by arrows) of sodium-carbonate evaporites gaylussite and/or pirssonite grew in carbonate mud and were later replaced by shortite post-burial. Northupite nodules (C, shown by arrows) grew in carbonate mud after brines become more alkaline and concentrated in magnesium. Row 3 is bedded cumulate evaporite, trona, characterized by crystals that precipitated at the air-water interface or in the water column, forming massive (E) and well-sorted microcrystalline (F) deposits on the basin floor. Row 4 is bottom-growth evaporite, composed of halite pseudomorphs replaced by trona (G) and halite (H). Bottom growth evaporites, in contrast with cumulates, grew in-place on the basin floor in concentrated, supersaturated bottom waters. They are characterized by large, clear crystals exhibiting competitive growth textures (G and H, shown by arrows).

calcium chloride brines (Na–K–Ca–Mg–Cl), sodium chloride brines (Na–K–Mg–SO_4–Cl), and alkaline brines (Na–K–CO_3–HCO_3–SO_4–Cl) (Fig. 3). As natural waters are concentrated during evaporation, Ca^{2+}, Mg^{2+}, and HCO_3^- are removed from the water during the precipitation of alkaline earth carbonates. If there is more $Ca^{2+} + Mg^{2+}$ than HCO_3^-, the resultant evolved water will be depleted in HCO_3^-. On the other hand, if there is more HCO_3^- than $Ca^{2+} + Mg^{2+}$, then the resultant water will become concentrated in HCO_3^-.

Dolomite mudstone (Fig. 2B) is abundant in the WPM in the Solvay S-34-1 core (Bradley 1931; Wolfbauer and Surdam, 1974; Smoot 1978; Smoot 1983; Klonowski et al., 2022) indicating supersaturation of the lake waters with respect to dolomite (Murphy et al., 2014). Saline

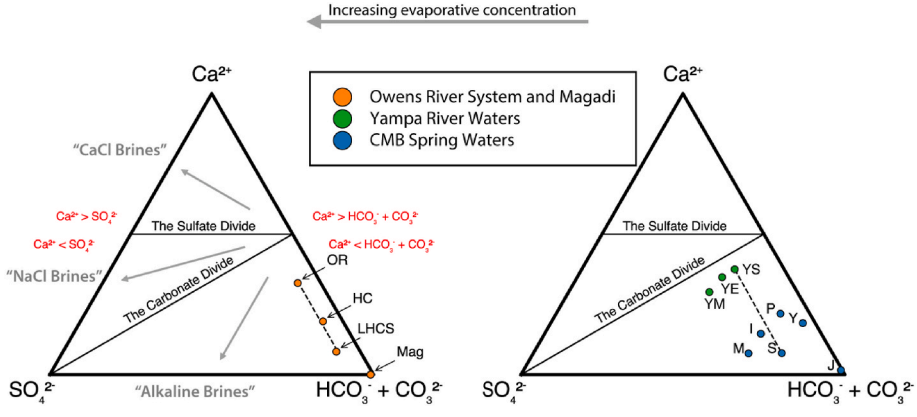

Fig. 3. Left: "Spencer Triangle" diagram showing the principle ionic divides, termed "the carbonate divide" and "the sulfate divide", potential water evolutive pathways (shown as arrows) and modern/Pleistocene analogues to Eocene Lake Gosiute brines and its hypothetical source waters. Waters that contain more carbonate alkalinity than calcium lie on the alkaline side of the "carbonate divide" and evolve into "alkaline" brines. Waters that contain more calcium than alkalinity encounter the sulfate divide after the carbonate divide. Brines containing more sulfate than calcium are termed "NaCl" or "neutral" brines, as brines that evolve along this pathway are relatively enriched in Na^+, SO_4^{2-} and Cl^-; brines containing more calcium than sulfate are termed "CaCl" brines because some of the calcium is charged balanced with Cl^-. Owens River (Hollett et al., 1991) is heavily influenced by springs charged with alkalinity from Long Valley Caldera volcanism. Little Hot Creek Springs (LHCS) (Sorey, 1985), which discharge into Hot Creek (HC) (Pretti and Stewart, 2002) and then into Owens River (OR), plot towards the alkaline vertex of the Spencer Triangle. Lake Magadi (Mag) surface brines (Jones et al., 1977; Renaut et al., 2021) are heavily fed by hot springs discharging directly into the basin. These waters are depleted in calcium and magnesium, and have relatively low sulfate due to sulfate reduction by bacteria in the water column (Renaut et al., 2021), so they plot close to the alkaline vertex of the Spencer Triangle.

Right: Modern Colorado Mineral Belt and vicinity soda spring compositions (Evans et al., 1986) (blue) (J = Juniper Spring; S = Steamboat Spring; I = Idaho Spring; M = Mineral Spring; P = Powder Horn Hot Spring; Y = Yellow Soda Spring). Modern Yampa River at Steamboat Springs (green) (YS) near Maybell (YM), and above Elkhead Creek (YE).

minerals in the WPM include trona, shortite, halite, northupite, and nahcolite (Fahey, 1939; Milton and Fahey, 1960). Shortite is a high temperature pseudomorphous replacement of gaylussite or pirssonite (Jagniecki et al., 2015). These minerals typically form large, randomly oriented blades in previously deposited carbonate mudstone (Fig. 2G). Northupite, a sodium-magnesium carbonate mineral, forms nodules in carbonate mudstone (Fig. 2C). Sulfide minerals (pyrite, pyrrhotite, marcasite) are also common in the Solvay S-34-1 core and the WPM in general (Tuttle and Goldhaber, 1993; Wiig et al., 1995; Klonowski et al., 2022), but sulfate minerals, a common constituent of many evaporite deposits in the geologic record, are notably absent (Dyni, 1996). The complete lack of sulfate minerals in the evaporite sequence and the presence of sulfide minerals embedded in mudstone facies suggests early sulfate-reduction, perhaps in the lacustrine water column, by salinity-stratification induced suboxia/anoxia as well as sulfate-reducing bacteria (Eugster, 1985; Wiig et al., 1995). Cumulate evaporites, predominantly composed of trona, form microcrystalline layered deposits within the WPM (Fig. 2E and 2F); small crystals grew at the air-water interface or within the water column and sank to the basin floor to accumulate. Bottom-growth evaporites, comprised of trona, trona pseudomorphs after halite, and halite, formed in-situ on the basin floor in highly saturated brines. They typically form large crystalline deposits growing upward into the water column (Fig. 2G and 2E).

The assemblage of minerals in the WPM falls in the "alkaline brines" end-member of chemical divides (Fig. 3) necessitating a parent brine in which $HCO_3^- + CO_3^{2-} > Ca^{2+}$. After the initial precipitation of dolomite, the resulting evolved brine is depleted in Ca^{2+} and enriched in alkalinity, allowing for the precipitation of the sodium-carbonate evaporite minerals in the lower WPM. Therefore, the parent waters that fed the GGRB during deposition of the WPM must have had relatively high alkalinity.

2.2. Magmatic and hydrothermal sources of excess carbonate alkalinity

Chemical weathering due to interactions between silicate minerals and meteoric waters has been proposed as a potential mechanism to supply Na^+ and HCO_3^- ions necessary to precipitate trona and other sodium-carbonate bearing minerals (Bradley and Eugster, 1969; Eugster and Hardie, 1975; Jones et al., 1977; Smith et al., 2008b). However, the absence of alkaline waters and trona deposits in many arid closed basins with volcanic bedrock suggests the need for excess alkalinity, beyond that supplied by chemical weathering at the Earth's surface (Earman et al., 2005; Lowenstein et al., 2017). Modern alkaline brines in Owens Lake and Searles Lake, California, USA, and in the Magadi Basin, Kenya, are associated with volcanism and hydrothermal activity that delivers extra alkalinity to these closed basins (Lowenstein et al., 2016, 2017; Renaut et al., 2021). Magmatism and faulting allow for the transfer of deeply-sourced CO_2 to more shallow aquifers (Earman et al., 2005). Rollback of the shallowly subducting Farallon plate during the late Cretaceous and early Eocene would have exposed large portions of the overlying hydrated North American lithosphere to hot asthenosphere, triggering widespread regional magmatism (Best et al., 2009; Humphreys, 2009; Smith et al., 2014).

The GGRB is located near several volcanic and plutonic provinces that were active during the early Eocene Epoch, including the Absaroka Volcanic Province, the Challis Volcanic Province, and the Colorado Mineral Belt, each of which could have supplied alkalinity to the GGRB if a riverine connection had existed (Fig. 1) (Lowenstein et al., 2017).

Absaroka volcanism was contemporaneous with deposition of the WPM (Smith et al., 2008a; Chetel et al., 2011). However, there is a lack of Absaroka- or Challis-derived volcanics within the WPM, likely due to diversion of drainage away from the GGRB during WPM deposition (Pietras and Carroll, 2006; Smith et al., 2008a; Chetel et al., 2011; Lowenstein et al., 2017; Honig et al., 2020). Most Challis volcanism, moreover, occurred after evaporite deposition of the lower WPM (Smith et al., 2008a, 2010; Chetel et al., 2011; Machlus et al., 2015). Smith et al. (2008a), Lowenstein et al. (2017), and Hammond et al. (2019) all concluded that inflow from the northern Absaroka and Challis volcanic provinces did not supply the excess alkalinity needed to form sodium carbonate evaporites in the WPM.

Another potential source of alkalinity to Eocene Lake Gosiute and the GGRB during the Early Eocene is magmatic and hydrothermal waters originating from the CMB to the southeast of the basin and transported by the Aspen paleoriver (Lowenstein et al., 2017; Hammond et al., 2019). The CMB is a narrow 400 km-long NE-trending strip of Cretaceous-Paleogene Laramide-aged shallow plutons and ore bodies emplaced above the east edge of the shallowly-subducting Farallon plate (Chapin, 2012). Magmatism and hydrothermal activity in the CMB occurred during multiple pulses from 75 to 0 Ma (Bookstrom, 1990), suggesting that it could have coincided with deposition of WPM evaporites. Crossbedded sandstone in the Cathedral Bluffs Member of the Wasatch Formation, laterally equivalent to the middle and upper WPM, at the southeast margin of the GGRB and northwest of the CMB, confirm northwestward flow into the basin during deposition of the WPM, consistent with the Aspen paleoriver hypothesis (Hammond et al., 2019). Additionally, lithic volcanic clasts and detrital zircon ages from WPM-equivalent siliciclastic sediments in the Washakie and Bridger Basins support CMB provenance (Hammond et al., 2019).

2.3. Modern hydrothermal springs as an Eocene analogue

As an additional test of whether the Aspen paleoriver could have supplied the alkalinity necessary to produce the evaporites observed in the WPM, we examine the chemical composition of modern soda springs from the CMB and vicinity. The monzonite plutons of the CMB exhibit a wide distribution of ages throughout the Cenozoic, documenting long-lived regional magmatism (Bookstrom, 1990; Chapin, 2012); modern hydrothermal springs, running through the same bedrock and charged by the same long-lived source of alkalinity as their ancient counterparts, are therefore reasonable analogues for ancient hydrothermal spring waters from the region. We use chemical modeling of these spring waters, at specified temperatures and pCO_2, to constrain inflow water chemistries, and add information about the environments existing in Lake Gosiute during evaporite deposition.

The chemical composition of soda springs from the CMB and vicinity is similar to the modern Owens River, California, USA (Hollett et al., 1991), the parent water of alkaline Searles Lake, and the hot spring waters of the Magadi Basin, Kenya (Jones et al., 1977; Renaut et al., 2021) (Fig. 2). The primary source of inflow to the Owens River is Sierra Nevada runoff, but a significant amount of solutes enter the Owens River from hydrothermal waters derived from the Long Valley Caldera (Pretti and Stewart, 2002; Lowenstein et al., 2016). Hot Creek, the second largest tributary of the Owens River, discharges alkaline water at temperatures of 28.4 °C and at a rate of 2.1 m^3s^{-1} into the Owens River (Pretti and Stewart, 2002). Nasikie Engida is a perennial alkaline lake in the Magadi Basin situated in a graben of the East African Rift in Kenya. The lake itself is recharged primarily by hydrothermal hot springs, discharging at temperatures up to 85 °C (Jones et al., 1977; Renaut et al., 2021). The Owens River is fresh water and represents a hydrothermal source water diluted by meteoric water derived from the Sierra Nevada. In contrast, Magadi Basin surface brines are concentrated and more evolved because they have undergone extensive evaporative concentration. Searles Lake and Lake Magadi both have sodium-carbonate evaporite minerals.

The major ion chemical composition of six modern soda springs from the CMB and vicinity is shown in Table 1 (from Evans et al., 1986). These springs were selected based on their highly alkaline nature (Fig. 3). Spring temperatures vary from 8° to 41 °C, with pH between 6.33 and 7.98. All the soda springs are dominated by Na–HCO_3–CO_3 and contain relatively low concentrations of Ca^{2+} and Mg^{2+}. Some have high Cl^- (Steamboat, Mineral, Yellow Soda) or high SO_4^{2-} (Steamboat, Idaho, Mineral). Carbon dioxide in these springs is thought to be derived from

Table 1
Water chemistry, isotopic composition, and gas volume percentages from modern Colorado Mineral Belt soda springs (adapted from Evans et al., 1986). For complete list of reported gases, see Table S1 in supplementary materials.

		Water Chemistry and Isotopic Composition													Gas Composition[b]	
ID	Name	T°C	pH	Ca^{2+}	Mg^{2+}	Na^{+}	K^{+}	CO_2[a]	HCO_3^-	Cl^-	SO_4^{2-}	SiO_2	$\delta^{18}O$	δD	$\delta^{13}C$ $SrCO_3$	$\delta^{13}C$ CO_2(g)	CH_4	CO_2
S	Steamboat Springs	26	6.55	110	31	2200	130	1670	3430	1400	540	24	−17.77	−136.7	−4.41	−7.3	0.02	98
J	Juniper Spring	37	7.98	3	0.33	470	2	21	1100	93	2	36	−18.93	−141.3	−2.21	0	77.18	1.41
I	Idaho Springs	50	6.33	130	39	515	73	1100	1470	68	400	68	−15.9	−117.4	−4.66	−6.22	<0.005	96.73
M	Mineral Spring	15	6.55	170	50	4550	120	2300	4570	3900	1400	10	−11.59	−108.5	−4.7	−8.5	0.01	97.85
Y	Yellow Soda Spring	8	6.64	240	150	1500	60	1600	3060	1300	120	78	−11.59	−86	−1.45	−7.07	0.005	91.97
P	Powder Horn Hot Spring	41	6.53	120	49	305	63	590	1170	120	120	80	−15.89	−127.1	−3.42	−6.27	0.01	96.3

Concentrations are reported in mg/L; isotopic compositions are reported in per mil. Oxygen and hydrogen isotopic values are reported using the SMOW standard; carbon isotopic values are reported using the PDB standard. Values listed are reported prior to removing sulfate (sulfate reduction) and charge balance.

[a] CO_2 (aq) concentration was measured as H_2CO_3.

[b] Gases were extracted into previously evacuated glass bulbs and analyzed via gas chromatography and mass spectrometry. Reported as percentages of total extracted gas.

the mantle or from metamorphism of marine carbonate rocks (Evans et al., 1986). All of these waters have relatively low dissolved CH_4 (<0.5% by volume of extracted gases analyzed) and high dissolved CO_2, with one exception, Juniper Spring (Table 1). The appreciable CH_4 and low SO_4^{2-} content, along with the slightly alkaline pH of Juniper Spring suggests sulfate reduction balanced by methane oxidation prior to discharge (Evans et al., 1986). There was likely a greater amount of methane relative to sulfate; nearly all sulfate was reduced with some methane left over. Evans et al. (1986) argue that Juniper Spring is the only water measured that emits appreciable amounts of ethane and methane; buried organic matter is likely responsible for the high methane content of Juniper Spring.

The similar chemical characteristics of modern CMB soda spring water chemistries and those of the Owens River and Magadi Basin hot springs support the hypothesis that the CMB-Aspen paleoriver could have supplied alkaline inflow water to the GGRB during the Early Eocene (Hammond et al., 2019). The minerals formed from CMB soda spring waters during evaporative concentration can be predicted from their major ion compositions. In order to precipitate the sodium-carbonate minerals of the lower WPM, CMB soda spring waters must lie in the alkaline section of the Spencer triangle (Fig. 3), which they do. Carbon isotope values from these modern Colorado soda springs indicate the possibility of a mantle origin for the elevated alkalinity in these waters (Evans et al., 1986).

3. Methods

Apt analogues for CMB source waters should produce the mineral sequences observed in the WPM. Evaporation of these waters (Table 1) can be simulated numerically to calculate the mass balance of chemical species and mineral phases by means of Gibbs free energy minimization. We used the chemical speciation program EQL/EVP (Risacher and Clement, 2001) to test whether CMB and nearby soda spring waters (Table 1) could produce the mineral sequences observed in lower WPM from the basin-center Solvay S-34-1 drill core of the Bridger Basin (Fig. 2).

Before they are input to EQL/EVP (Risacher and Clement, 2001), major ion concentrations from CMB soda springs are converted from mg/L (reported in Evans et al., 1986) to molarities (mol/L). To simulate syndepositional sulfate reduction in Lake Gosiute, sulfate was removed from each input water and balanced by addition of a charge-equivalent amount of bicarbonate alkalinity, consistent with the sulfate reduction reaction of Goldhaber (2003):

$$SO_4^{2-} + 2CH_2O = H_2S + 2HCO_3^-$$

In this case, 2 mol of bicarbonate are produced from every mole of sulfate reduced, which raises the alkalinity of the water even higher. Goldhaber (2003) argued that bacterial dissimilatory sulfate reduction is a significant component of the global sulfur cycle. This process occurs in modern Lake Nasikie Engida in the Magadi Basin, Kenya (Renaut et al., 2021). A sulfate reduction step is done because there are no sulfate-bearing minerals in the WPM, indicating that the SO_4^{2-} concentration in Lake Gosiute was low. Instead, the WPM contains pyrite, marcasite and pyrrhotite, all with reduced sulfur.

All waters are charge-balanced by adjusting the cations and anions to ensure electrical neutrality. EQL/EVP first calculates the saturation state and initial precipitation of minerals before evaporation. Next, stepwise evaporation of waters is simulated by incrementally removing H_2O from the system and recalculating the saturation state of mineral phases in the system. The original source code of EQL/EVP was rewritten to forward-model the evaporation of an aliquot of water, of specified input chemistry, to high ionic strength utilizing the Pitzer ion-interaction model to calculate activity coefficients (Risacher and Clement, 2001). The program was modified for this study to run iterative simulations at a wide range of temperatures and pCO_2 values. The result data files were

evaluated for the first precipitation of each mineral at the particular temperature and pCO_2 of that simulation. Those data were compiled at all simulated temperature and pCO_2 conditions to create a conservative model of chemical speciation and mineral precipitation for each tested inflow water. Modeled mineral sequences were then compared to the mineral sequences observed in the Solvay S-34-1 core.

The evaporation of modern CMB spring waters and mineral precipitation was simulated at temperatures 0-50 °C and pCO_2 values from 400 to 2000 ppm to consider all possible paleolake temperatures and Eocene CO_2 concentrations (Jagniecki et al., 2015; Demicco and Lowenstein, 2020). The paragenesis of WPM evaporite minerals may be deduced from observation of the depositional and diagenetic features preserved in the Solvay core, summarized in Fig. 3 (Jagniecki and Lowenstein, 2015; Klonowski et al., 2022). EQL/EVP allows users to specify "closed-" or "open-system" behavior before running simulations. In this context, "closed-system" behavior allows precipitated salts to be dissolved or back-reacted with the evaporating brine during the entire simulation. In contrast, "open-system" behavior removes precipitated minerals from the system so they are not available to back react with the evolving brine. Closed and open behaviors were initially considered when simulating the evaporation of CMB inflow waters; however, "closed system" conditions are needed to account for the diagenetic minerals gaylussite and pirssonite (now shortite) because they form via reaction between primary carbonate minerals (i.e., calcite) and residual brines (Olson and Lowenstein, 2021; Klonowski et al., 2022). Shortite is not known to form naturally in modern lakes. However, the formation of shortite from pirssonite in the Na_2CO_3–$CaCO_3$–H_2O system has been experimentally determined to occur above 55 ± 2 °C (Jagniecki et al., 2013). Shortite occurs in the lower WPM as a pseudomorph after pirssonite or gaylussite, both of which form displacive crystals in carbonate mud facies (Jagniecki et al., 2013; Jagniecki and Lowenstein, 2015; Klonowski et al., 2022). Therefore, the simulated precipitation of pirssonite and/or gaylussite is considered to be analogous to the observation of shortite in WPM deposits. In addition, northupite ($Na_3Mg(CO_3)_2Cl$) commonly occurs with shortite as diagenetic, displacive nodules in the carbonate muds of this depositional motif (Klonowski et al., 2022).

Continued evaporative concentration of the lake brine would produce trona. Trona primarily occurs in the Solvay S-34-1 core as a cumulate deposit (Lithofacies 3, Fig. 2), indicating precipitation in the water column and accumulation at the bottom of the lake (Klonowski et al., 2022). The fourth and final depositional motif present in the Solvay core is bottom-growth trona and halite (NaCl) (Lithofacies 4, Fig. 2) (Klonowski et al., 2022). Bedded trona and halite in the lower WPM exhibit cumulate and bottom-growth structures, which indicate formation in the water column and brine bottom, respectively, during the later stages of evaporative concentration and brine evolution (Klonowski et al., 2022) (Fig. 2).

Table 2
Names and formulas of evaporite minerals mentioned in this manuscript.

Mineral	Formula
Calcite	$CaCO_3$
Dolomite	$CaMg(CO_3)_2$
Gaylussite	$Na_2Ca(CO_3)_2•5H_2O$
Pirssonite	$Na_2Ca(CO_3)_2•2H_2O$
Shortite	$Na_2Ca_2(CO_3)_3$
Northupite	$Na_3Mg(CO_3)_2Cl$
Trona	$Na_3H(CO_3)_2•2H_2O$
Nahcolite	$NaHCO_3$
Natron	$Na_2CO_3•10H_2O$
Halite	NaCl
Sylvite	KCl

4. Results

The simulated evaporation of the various CMB soda spring waters (Table 1) produces unique sequences and amounts of evaporite minerals (Table 2). Starting from the initial sulfate-reduced and charge-balanced input water, all six CMB spring waters are supersaturated with respect to alkaline earth carbonates, calcite and dolomite. Such early precipitation of Ca–Mg-carbonate matches the expected relatively low salinity lithology in the Solvay core: carbonate mudstone (Lithofacies 1, Fig. 2).

Under closed-system equilibrium conditions, previously precipitated calcite back-reacts with the evolved water to form the Na–Ca–CO_3 minerals gaylussite ($Na_2Ca(CO_3)_2•5H_2O$) (temperatures below 27 °C) or pirssonite ($Na_2Ca(CO_3)_2•2H_2O$) (temperatures above 27 °C), resembling the second depositional motif in the lower WPM: displacive evaporite minerals formed in mud by back-reaction with alkaline earth carbonate minerals (Lithofacies 2, Fig. 2). In most simulations, gaylussite and pirssonite precipitate immediately before or after northupite ($Na_3Mg(CO_3)_2Cl$). The order in which they precipitate in simulation depends on the relative amount of Mg and Cl in the brine; waters relatively enriched in magnesium and chloride (Mineral Spring, Yellow Soda Spring, and Powder Horn Hot Spring) precipitate northupite and then pirssonite at 1200 ppm pCO_2 and 30 °C, whereas waters with less Mg and Cl (Steamboat Springs, Juniper Spring, and Idaho Springs) precipitate pirssonite before northupite (Table 2). The water most depleted in Mg, Juniper Spring, does not precipitate northupite until after the onset of trona precipitation.

Trona occurs as a primary precipitate in simulations, rather than a back-reacted precipitate formed from previously deposited minerals, as would be expected for cumulate evaporites (Lithofacies 3, Fig. 2), which crystallize at the air-water interface and then sink through the water column. Similarly, halite occurs in simulation as a primary precipitate, which is consistent with bottom-growth evaporite deposits (Lithofacies 4, Fig. 2), as these deposits grow at the bottom of the water column rather than in brine-saturated muds.

The mineral sequences that most closely match the lithofacies in the Solvay core (Fig. 2) are produced by evaporation of Steamboat Springs and Mineral Spring waters at 1200 ppm CO_2 and 30 °C (Table 2): primary alkaline earth carbonates (calcite and/or dolomite), Na–Ca-carbonate (pirssonite) formed by reaction of brine with previously precipitated calcite, followed by northupite, trona, and halite (Fig. 4). Evaporation of water from Yellow Soda Spring also produces a close match to the observed mineral sequence of the Solvay core, but northupite precipitates before pirssonite in this simulation. Notably, halite precipitation does not occur during simulated evaporation of Idaho Springs and Powder Horn Hot Spring waters (Fig. 5).

At the onset of simulation ("1" on Fig. 4), precipitation of alkaline earth carbonate, in this case, calcite, removes most calcium from the water. The water must then undergo significant evaporative concentration before the next mineral, pirssonite, begins to precipitate at the expense of calcite ("2" on Fig. 4). Steamboat Springs water must be concentrated 44 times before pirssonite precipitation. As evaporation of Steamboat Springs water takes place, all ions not involved in mineral precipitation exhibit conservative behavior. This can be seen in Fig. 4 by the parallel lines, indicating conservative behavior of Na^+, K^+, Mg^{2+}, and Cl^-, until pirssonite forms. Alkalinity appears to behave conservatively because it is several orders of magnitude higher in concentration than Ca^{2+}. Thus, only a small amount of the total alkalinity is consumed during evaporative concentration between initial supersaturation with calcite and precipitation of pirssonite.

As shown in Fig. 4, northupite precipitates immediately after pirssonite, which consumes most magnesium and a nominal amount of alkalinity and sodium from the brine. Northupite, a Na–Mg–CO_3–Cl mineral, is predicted to form in simulations in which dolomite is removed from the thermodynamic database. That is because removal of dolomite from the database allows Mg^{2+} to become concentrated in the brine during evaporation. Northupite, however, occurs in the Solvay

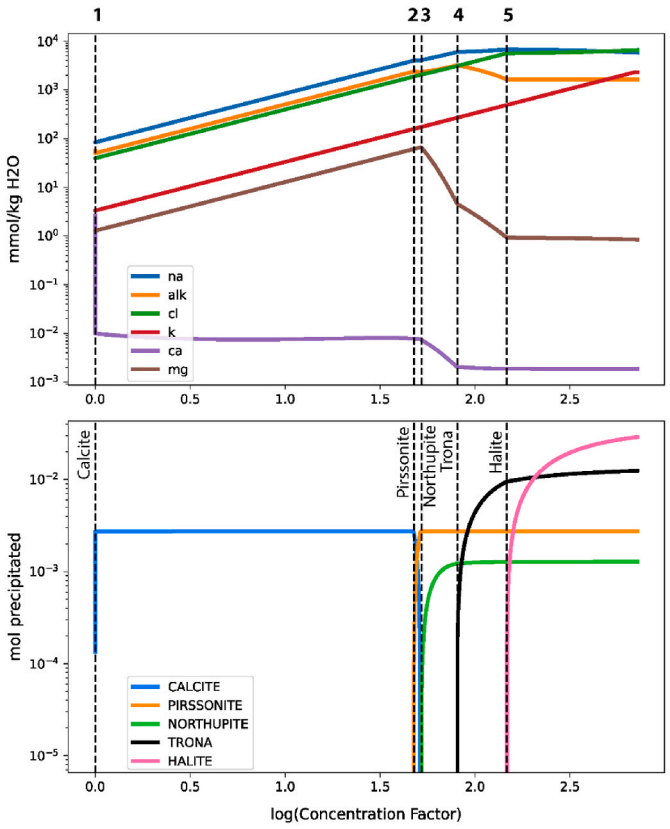

Fig. 4. Simulated stepwise evaporation of Steamboat Springs water: T = 30 °C, pCO_2 = 1200 ppm, "closed system" conditions. Sulfate was removed and balanced by addition of $2HCO_3^-$ because brines in the Bridger Basin were depleted in SO_4^{2-}, due to syndepositional sulfate reduction, as occurs today in the Magadi Basin (Renaut et al., 2021). Note the precipitation of calcite at low salinity/evaporative concentration (marked by the dashed line labeled "1"). As the Steamboat Springs water is concentrated, pirssonite forms from back reaction of the residual brine with calcite ("2"). At temperatures less than 27 °C, gaylussite forms instead of pirssonite. With further evaporation, northupite ("3"), trona ("4"), and halite ("5") precipitate.

core as diagenetic nodules in carbonate mudstone (Klonowski et al., 2022), indicating early diagenetic crystallization.

With further evaporative concentration, trona precipitates ("3" on Fig. 4, at a concentration factor of 73), consuming alkalinity and sodium. Finally, halite precipitates ("4 on Fig. 4", at a concentration factor of 147), consuming sodium and chloride from the water. Chloride behaves conservatively until halite saturation. Because no K-bearing minerals form until the very end of the simulation (after halite precipitation), potassium behaves conservatively for the vast majority of the simulation. The evaporation of Steamboat Springs water removes Ca^{2+} and Mg^{2+} during precipitation of calcite, pirssonite and northupite, and produces a concentrated brine rich in Na^+ K^+, alkalinity, and Cl^-.

5. Discussion

5.1. Mineral paragenesis in simulated and observed sequences

The results of the simulated evaporation of modern Colorado soda springs allows for the direct comparison between hydrothermal source water analogues and the observed WPM mineral parageneses in the Solvay S-34-1 core. The close match between the mineral sequences produced by simulated evaporation of Steamboat Springs, Mineral Spring, and Yellow Soda Spring waters (Table 3; Fig. 5) and observed mineral sequences (Fig. 2) provides new insights into potential hydrothermal inflow sources to Eocene Lake Gosiute as well as the evolution of the lake brine as it underwent evaporative concentration.

One difference between the observed and simulated mineral sequences is the alkaline earth carbonate precipitate. Whereas calcite is common as the initial primary precipitate in many simulations, dolomite is the only alkaline earth carbonate in the Solvay core. Other primary carbonates (calcite, aragonite), if precipitated, must have been subsequently dissolved or reacted to form another mineral. Calcite occurs in marginal WPM deposits, close to where streams entered the basin from the Uinta Mountains, suggesting that Ca^{2+}-bearing inflow waters precipitated calcite when they mixed with alkaline lake waters (Smith et al., 2015; Smoot, 1978). In addition, dolomite and calcite both occur in areas north of the basin-center Solvay core location. Calcite, for example, is a minor mineral in the ERDA Blacks Fork #1 core and a major phase in the US ERDA White Mountain #1 core further to the north (Baddouh et al., 2017).

Another possibility is that calcite/aragonite were lost by reaction with connate waters to form gaylussite or pirssonite (Fig. 4), now dehydrated to shortite. The evidence for this reaction is the displacive diagenetic textures of gaylussite/pirssonite pseudomorphs in the carbonate mudstone facies (Lithofacies 2, Fig. 2). Displacive growth of gaylussite/pirssonite involves the reaction between previously deposited carbonate mud and concentrated brine. The displacive nature of the gaylussite/pirssonite pseudomorphs is therefore consistent with evaporation models, in which calcite/aragonite back-react, in situ, with concentrated brines in sediment pores. Support for this interpretation comes from late Pleistocene subsurface sediments in Searles Lake, California. There, layers of carbonate mud are predominantly dolomite, with abundant displacive crystals of gaylussite (Olson and Lowenstein, 2021). Rarely, aragonite and calcite occur in distinctive monomineralic laminae, such as in the late Pleistocene Parting Mud, ~22–25 m below the surface (Olson and Lowenstein, 2021). But no gaylussite or pirssonite occur with the calcite/aragonite laminae of the Parting Mud, suggesting they are unreacted primary carbonate vestiges.

5.2. Implications for alkalinity and regional climate during the Early Eocene

The evaporites in the lower WPM were deposited during a period of significant global warmth, the EECO (Zachos et al., 2001, 2008). The composition of these chemogenic sediments reflects parent water chemistry, temperature, and pCO_2 in the lake at the time of deposition. Constraining the chemistry of the parent water and particularly the source of excess alkalinity responsible for this massive sodium-carbonate deposit is of interest for understanding Lake Gosiute during the Early Eocene and how it responded to global warmth.

Modern soda springs from northwestern Colorado are alkaline and CO_2-charged. The CO_2 of these soda springs may be mantle-derived (Evans et al., 1986), indicating a long-lived regional source of elevated alkalinity. Modern soda springs therefore represent a suitable potential proxy for Eocene soda springs, charged with CO_2 from the mantle, flowing through the same bedrock. Computer-simulated evaporation of these waters, in particular Steamboat Springs, Mineral Spring, and Yellow Soda Spring, produces the mineral sequences observed in the lower WPM.

The simulated evaporation of modern Colorado soda spring waters at various temperatures and pressures provides new insights into the temperature, pCO_2, and salinity of Lake Gosiute at the time of deposition of the lower WPM. Gaylussite-pirssonite and trona-natron-nahcolite are sensitive to the temperature and pCO_2 of the lake brine and thus provide constraints on the hydroclimatic conditions at the time of deposition (Jagniecki et al., 2015). At pCO_2 of 400 ppm, for example, the trona-nahcolite boundary occurs at ~15 °C; below this temperature, nahcolite is the primary precipitate, and above 15 °C, trona precipitates (Fig. 5). At higher pCO_2, the temperature of the trona-nahcolite boundary increases.

The gaylussite-pirssonite equilibrium boundary occurs at ~27 °C;

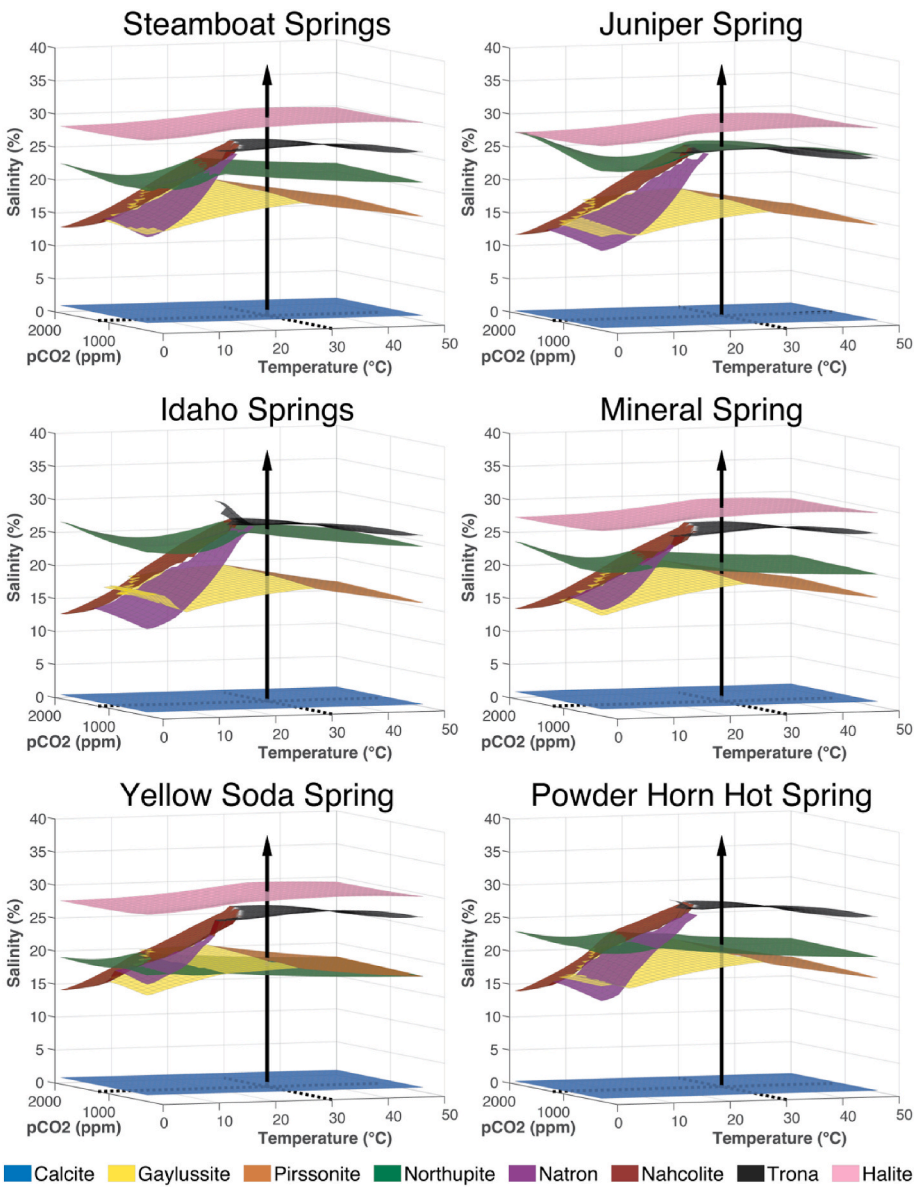

Fig. 5. First precipitation surfaces of minerals from simulated evaporation of modern Colorado Mineral Belt soda springs waters, calculated at temperatures 0-50 °C and pCO_2 concentrations of 400–2000 ppm. Simulations used "closed-system" equilibrium conditions, such that previously precipitated minerals (calcite) are retained in the simulation and are allowed to dissolve/back-react with the residual brine to form gaylussite and pirssonite (replaced by shortite during burial diagenesis (see Jagniecki et al., 2013). Vertical arrows illustrate the evaporation pathway/simulation conditions utilized in Table 3 and Fig. 4 (1200 ppm pCO_2 and 30 °C).

Table 3
Results of simulated evaporation of soda spring waters from modern Colorado Mineral Belt and vicinity. Mineral sequences are plotted on Fig. 5.

Name	Predicted Mineral Sequence at 30 °C, 1200 ppm pCO_2
Steamboat Springs	Calcite – Pirssonite – Northupite – Trona – Halite
Juniper Spring	Calcite – Pirssonite – Trona – Northupite – Halite
Idaho Springs	Calcite – Gaylussite – Pirssonite – Northupite – Trona – Sylvite
Mineral Spring	Calcite – Pirssonite – Northupite – Trona – Halite
Yellow Soda Spring	Calcite – Northupite – Pirssonite – Trona – Halite
Powder Horn Hot Spring	Calcite – Pirssonite – Northupite – Trona – Sylvite

below this temperature, gaylussite precipitates, which may later dehydrate to pirssonite. At or above 27 °C, pirssonite precipitates and gaylussite does not form at all. The gaylussite-pirssonite phase equilibria, paired with the stability of trona and nahcolite, further constrain the maximum bottom-water temperature and pCO_2 estimates for those portions of the lower WPM in which gaylussite pseudomorphs and trona occur (Fig. 6). For deposits with gaylussite as the initial sodium-calcium-carbonate, and with trona, water temperatures are constrained to 15-27 °C and partial pressure of CO_2 to <1200 ppm. If, however, the initial Na–Ca-carbonate mineral was pirssonite, then lake waters were >27 °C.

These pCO_2 and temperature ranges agree with estimates from previous studies. Jagniecki et al. (2015), using the nahcolite proxy, estimated atmospheric pCO_2 values of 680–1260 ppm and lake water temperatures of 19.5–34 °C from contemporaneous evaporites in the neighboring Piceance Creek Basin of Colorado. LaClair and Lowenstein (2010) estimated lake water temperature during the early Eocene to be 21-28 °C from fluid inclusion microthermometry experiments conducted on Piceance Creek Basin halites. These temperature ranges also agree with those obtained from leaf fossils in the GGRB of 23 °C and 19.6 °C from ~50 Ma (Wilf, 2000). Lower temperature ranges were obtained from pedogenic soil carbonates in floodplain deposits on the margin of the GGRB (Hyland and Sheldon, 2013).

Equilibrium models of lake water evaporation and mineral precipitation also provide quantitative information about lake salinity. First precipitation of gaylussite, pirssonite, trona, and halite occurs at discrete salinities which are more or less independent of temperature and pCO_2 (Fig. 5). As such, these minerals provide semi-quantitative estimates of salinity of the lake brine at various points during deposition (Table 4). The average salinity at which gaylussite/pirssonite, trona, and halite

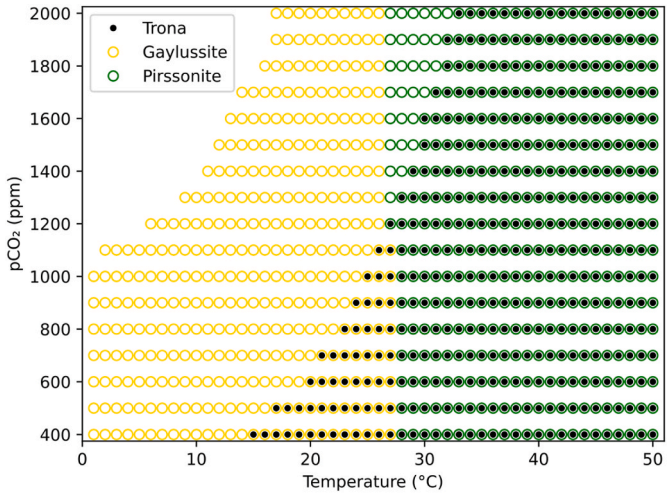

Fig. 6. Co-precipitation of gaylussite, pirssonite, and trona from simulated evaporation of Steamboat Springs water at temperatures of 0-50 °C and pCO_2 of 400–2000 ppm. Yellow circles represent simulations which initially yield gaylussite (later to be replaced by pirssonite), green circles represent simulations which initially yield pirssonite (no gaylussite at any point of simulation), and black dots represent simulations which yield trona. Intersection of black dots and green or yellow circles indicate simulations in which trona and gaylussite or trona and pirssonite precipitate. At temperatures at or above 27 °C, pirssonite forms instead of gaylussite as the initial precipitate; at temperatures below 27 °C, gaylussite initially precipitates, but is later replaced by pirssonite under "closed system" conditions. Note the small subset of simulations that produce gaylussite and trona (pCO_2 < 1200 ppm and temperatures of 15-27 °C).

Table 4
Mean salinities and standard deviations at first precipitation of various minerals from simulated evaporation of modern soda spring waters, from the Colorado Mineral Belt and vicinity, at temperatures of 0-50 °C and pCO_2 of 400–2000 ppm.

Water	Mineral	Mean Salinity	Standard Deviation
Steamboat Springs	Gaylussite + Pirssonite	17.53%	1.12%
	Northupite	21.71%	0.67%
	Trona	25.75%	0.75%
	Halite	29.41%	0.73%
Juniper Spring	Gaylussite + Pirssonite	16.22%	1.01%
	Northupite	24.84%	1.04%
	Trona	25.05%	0.92%
	Halite	28.55%	0.78%
Idaho Springs	Gaylussite + Pirssonite	17.68%	0.94%
	Northupite	25.16%	0.77%
	Trona	26.69%	1.14%
Mineral Spring	Gaylussite + Pirssonite	18.31%	1.11%
	Northupite	21.13%	0.61%
	Trona	26.21%	0.68%
	Halite	28.66%	0.77%
Yellow Soda Spring	Gaylussite + Pirssonite	18.82%	0.87%
	Northupite	18.47%	0.53%
	Trona	26.46%	0.67%
	Halite	28.94%	0.76%
Powder Horn Hot Spring	Gaylussite + Pirssonite	19.24%	1.1%
	Northupite	21.71%	0.69%
	Trona	27.13%	0.95%

precipitated in the simulated evaporation of Steamboat Springs water, for example, is 17.5 ± 2.2%, 25.6 ± 1.5%, and 29.4 ± 1.5%, respectively. These salinities are relatively consistent among all simulated waters. Such high salinities suggest that the bulk of the lower WPM was deposited in a hypersaline lake setting.

6. Conclusions

The simulated evaporation of modern Colorado soda spring waters produces a mineral sequence similar to that observed in the basin-center Solvay S-34-1 core. The CMB may have been active during the early Eocene, and modern CMB soda spring waters, derived from the same magmatic provenance and flowing through the same bedrock, may be a suitable analog for Eocene CMB spring waters that contributed alkalinity to the GGRB. Fluvial facies to the southeast of the GGRB have west/northwest paleocurrent indicators, which confirms a fluvial connection between the CMB and the GGRB (Hammond et al., 2019). Therefore, soda spring waters of the CMB may have supplied alkalinity to the river system that delivered water to the GGRB at the time of deposition of the lower WPM evaporite.

The modeled evaporation of various modern CMB spring waters provides new insights into the composition of ancient parent water inflow to the GGRB. Modeled salt precipitation compared with the mineral sequences found in the basin-center Solvay S-34-1 core offers new insights into the regional environmental conditions at the time of deposition. This study focused on six modern CMB spring waters (Table 1) (Evans et al., 1986) as potential parent water proxies. Of these six waters, the simulated evaporation of Steamboat Springs water (Fig. 5) yielded the closest match to the mineral sequence found in the lower WPM of the Solvay core (Fig. 2). These simulations support the hypothesis that inflow waters derived from the CMB and vicinity and delivered to the GGRB by the Aspen paleoriver could have supplied the excess alkalinity needed to precipitate the sodium-carbonate evaporites of the lower WPM of the Green River Formation in the Bridger Basin of Wyoming.

Mineral equilibria, assuming gaylussite as the initial sodium-calcium-carbonate, and with trona, constrain lake water temperatures to 15-27 °C and partial pressure of CO_2 to <1200 ppm. If pirssonite was the initial Na–Ca-carbonate, then lake waters were >27 °C. These pCO_2 and temperature ranges agree closely with estimates from previous studies. Simulated evaporation of Steamboat Springs water shows that gaylussite/pirssonite, trona, and halite precipitated at salinities of 18.7 ± 2.2%, 26.6 ± 1.4%, and 29.4 ± 1.5%, respectively. These salinities suggest a hypersaline lake setting for the bulk of the lower WPM.

Declaration of competing interest

The authors declare that they have no known competing financial interests or personal relationships that could have appeared to influence the work reported in this paper.

Data availability

Data will be made available on request.

Acknowledgements

We thank Matteo Paperini and Solvay Chemicals, Inc. for their contribution of the Solvay S-34-1 core. We thank Robert V. Demicco for his insights and expertise in modeling carbonate and evaporite deposition. We thank the staff at LacCore National Lacustrine Core Facility at the University of Minnesota, Minneapolis for processing and storage of the core: Kristina Brady Shannon, Anders Noren, Ryan O'Grady, Amy Myrbo, Mark Shapley, Alex Stone and Jessica Heck. We gratefully acknowledge Andrew Walters, Shlomo Honig, Isaac Sageman, for their assistance in the preparation, imaging, and logging of the core. We thank

David Tuttle for core and thin section photomicrographs reproduced in this manuscript. This study received financial support from the National Science Foundation Integrated Earth Systems Program (NSF-EAR 1812741; NSF-EAR 1813278; NSF-EAR 1813350).

Appendix A. Supplementary data

Supplementary data to this article can be found online at https://doi.org/10.1016/j.apgeochem.2023.105597.

References

Aswasereelert, W., Meyers, S.R., Carroll, A.R., Peters, S.E., Smith, M.E., Feigl, K.L., 2013. Basin-Scale Cyclostratigraphy of the Green River Formation, Wyoming, vol. 125. Geological Society Of America Bulletin, pp. 216–228. https://doi.org/10.1130/B30541.1.

Baddouh, M., Carroll, A.R., Meyers, S.R., Beard, B.L., Johnson, C.M., 2017. Chronostratigraphic correlation of lacustrine deposits using $^{87}Sr/^{86}Sr$ ratios, Eocene Green River Formation, Wyoming, USA. J. Sediment. Res. 87, 406–423.

Best, M.G., Barr, D.L., Christiansen, E.H., Gromme, S., Deino, A.L., Tingey, D.G., 2009. The Great Basin Altiplano during the middle Cenozoic ignimbrite flareup: insights from volcanic rocks. Int. Geol. Rev. 51, 589–633. https://doi.org/10.1080/00206810902867690.

Bohacs, K.M., Carroll, A.R., Neal, J.E., Mankiewicz, P.J., Gierlowski-Kordesch, E., Kelts, K., 2000. Lake-basin type, source potential, and hydrocarbon character: an integrated sequence-stratigraphic-geochemical framework: lake basins through space and time. AAPG Stud. Geol. 46, 3–34.

Bookstrom, A.A., 1990. Igneous rocks and carbonate-hosted ore deposits of the central Colorado mineral Belt. In: Beaty, D.W., Landis, G.P., Thompson, T.B. (Eds.), Carbonate-Hosted Sulfide Deposits of the Central Colorado Mineral Belt. Economic Geology Publishing Company, Economic Geology Monograph 7, pp. 45–65. https://doi.org/10.5382/Mono.07.04.

Bradley, W.H., 1964. Geology of Green River Formation and Associated Eocene Rocks in Southwestern Wyoming and Adjacent Parts of Colorado and Utah: Professional Paper USGS Numbered Series 496-A. https://pubs.er.usgs.gov/publication/pp496A.

Bradley, W.H., 1931. Origin and Microfossils of the Oil Shale of the Green River Formation of Colorado and Utah. Professional Paper USGS Numbered Series 168. https://pubs.er.usgs.gov/publication/pp168.

Bradley, W.H., Eugster, H.P., 1969. Geochemistry and Paleolimnology of the Trona Deposits and Associated Authigenic Minerals of the Green River Formation of Wyoming. Professional Paper USGS Numbered Series 496-B. http://pubs.er.usgs.gov/publication/pp496B. May 2019.

Carroll, A.R., Bohacs, K.M., 1999. Stratigraphic classification of ancient lakes: balancing tectonic and climatic controls. Geology 27, 99–102.

Chapin, C.E., 2012. Origin of the Colorado mineral Belt. Geosphere 8, 28–43. https://doi.org/10.1130/GES00694.1.

Chetel, L.M., Janecke, S.U., Carroll, A.R., Beard, B.L., Johnson, C.M., Singer, B.S., 2011. Paleogeographic Reconstruction of the Eocene Idaho River, North American Cordillera, vol. 123. Geological Society of America Bulletin, pp. 71–88. https://doi.org/10.1130/B30213.1.

Culbertson, W.C., 1961. Stratigraphy of the Wilkins Peak Member of the Green River Formation, Firehole Basin Quadrangle, Wyoming: Professional Paper USGS Numbered Series 424-D, pp. 170–173. https://pubs.er.usgs.gov/publication/pp424D.

Demicco, R.V., Lowenstein, T.K., 2020. When "Evaporites" Are Not Formed by Evaporation: the Role of Temperature and pCO_2 on Saline Deposits of the Eocene Green River Formation, vol. 132. Geological Society of America Bulletin, Colorado, USA, pp. 1365–1380. https://doi.org/10.1130/B35303.1.

Dickinson, W.R., Klute, M.A., Hayes, M.J., Janecke, S.U., Lundin, E.R., McKITTRICK, M.A., Olivares, M.D., 1988. Paleogeographic and paleotectonic setting of Laramide sedimentary basins in the central Rocky Mountain region. Geol. Soc. Am. Bull. 100, 1023–1039.

Drever, J.I., 1982. The Geochemistry of Natural Waters. Prentice-Hall, Englewood Cliffs, N.J, p. 388.

Dyni, J.R., 1996. Sodium Carbonate Resources of the Green River Formation. U. S. Geological Survey Open-File Report, pp. 96–729.

Earman, S., Phillips, F.M., McPherson, B.J.O.L., 2005. The role of "excess" CO_2 in the formation of trona deposits. Appl. Geochem. 20, 2217–2232. https://doi.org/10.1016/j.apgeochem.2005.08.007.

Eugster, H.P., 1985. Oil shales, evaporites and ore deposits. Geochem. Cosmochim. Acta 49, 619–635. https://doi.org/10.1016/0016-7037(85)90158-9.

Eugster, H.P., Hardie, L.A., 1975. Sedimentation in an Ancient Playa-Lake Complex: the Wilkins Peak Member of the Green River Formation of Wyoming, vol. 86. Geological Society of America Bulletin, pp. 319–334. https://doi.org/10.1130/0016-7606(1975)86<319:SIAAPC>2.0.CO;2.

Evans, W.C., Presser, T.S., Barnes, I., 1986. Selected Soda Springs of Colorado and Their Origins: US Geological Survey Water Resources Paper 2310, pp. 45–52.

Fahey, J.J., 1939. Shortite, a new carbonate of sodium and calcium1. Am. Mineral. 24, 514–518.

Goldhaber, M.B., 2003. Sulfur-rich sediments. In: Holland, H.D., Turekian, K.K. (Eds.), Treatise on Geochemistry. Pergamon, Oxford, pp. 257–288. https://doi.org/10.1016/B0-08-043751-6/07139-5.

Hammond, A.P., Carroll, A.R., Parrish, E.C., Smith, M.E., Lowenstein, T.K., 2019. The Aspen paleoriver: linking Eocene magmatism to the world's largest Na-carbonate evaporite (Wyoming, USA). Geology 47, 1020–1024. https://doi.org/10.1130/G46419.1.

Hardie, L.A., Eugster, H.P., 1970. The Evolution of Closed-Basin Brines: Mineralogical Society of America, Special Paper 3, pp. 273–290.

Hollett, K.J., Danskin, W.R., McCaffrey, W.F., Walti, C.L., 1991. Geology and Water Resources of Owens Valley, 2370B. Water Supply Paper Report, California, p. 77. https://doi.org/10.3133/wsp2370B.

Honig, S., Carroll, A.R., Gygi, D.J., Smith, M.E., 2020. Early Eocene drainage evolution of the Idaho paleoriver, Green River Basin, Wyoming. In: Abstracts with Programs, vol. 52. Geological Society of America, p. 6. https://doi.org/10.1130/abs/2020AM-357639.

Humphreys, E., 2009. Relation of flat subduction to magmatism and deformation in the western United States. In: Kay, S.M., Ramos, V.A., Dickinson, W.R. (Eds.), Backbone of the Americas: Shallow Subduction, Plateau Uplift, and Ridge and Terrane Collision. Geological Society of America Memoir 204, pp. 85–98. https://doi.org/10.1130/2009.1204(04.

Hyland, E.G., Sheldon, N.D., 2013. Coupled CO_2-climate response during the early Eocene climatic Optimum. Palaeogeogr. Palaeoclimatol. Palaeoecol. 369, 125–135. https://doi.org/10.1016/j.palaeo.2012.10.011.

Jagniecki, E.A., Jenkins, D.M., Lowenstein, T.K., Carroll, A.R., 2013. Experimental study of shortite ($Na_2Ca_2(CO_3)_3$) formation and application to the burial history of the Wilkins Peak member, Green River Basin. Wyoming, USA: Geochem. Cosmochim. Acta 115, 31–45. https://doi.org/10.1016/j.gca.2013.04.005.

Jagniecki, E.A., Lowenstein, T.K., 2015. Evaporites of the Green River Formation, bridger and piceance Creek basins: deposition, diagenesis, paleobrine chemistry, and Eocene atmospheric CO_2. In: Smith, M.E., Carroll, A.R. (Eds.), Stratigraphy and Paleolimnology of the Green River Formation, vol. 1. Springer Netherlands, Western USA, Dordrecht, pp. 277–312. https://doi.org/10.1007/978-94-017-9906-5_11.

Jagniecki, E.A., Lowenstein, T.K., Jenkins, D.M., Demicco, R.V., 2015. Eocene atmospheric CO_2 from the nahcolite proxy. Geology 43, 1075–1078. https://doi.org/10.1130/G36886.1.

Jones, B.F., Eugster, H.P., Rettig, S.L., 1977. Hydrochemistry of the lake Magadi basin, Kenya. Geochem. Cosmochim. Acta 41, 53–72. https://doi.org/10.1016/0016-7037(77)90186-7.

Klonowski, E., Lowenstein, T.K., Carroll, A.R., Smith, M.E., Paperini, M., Pietras, J.T., 2022. Recurring lacustrine depositional successions in the Wilkins Peak member, Green River Formation: the basin-center evaporite perspective. In: Vanden Berg, Michael D., Riley, Brinkerhoff, Birdwell, Justin E., Jagniecki, Elliot A., Birgenheier, Lauren P. (Eds.), The Lacustrine Green River Formation: Hydrocarbon Potential and Eocene Climate Record, vol. 50. Utah Geological Survey Publication, p. 23. https://doi.org/10.31711/ugap.v50i.116.

LaClair, D., Lowenstein, T., 2010. Using microthermometry, laser Raman spectroscopy and evaporites to reconstruct the paleoclimate of the Eocene Green River Formation, Colorado, USA. In: 10th Biennial Pan-American Current Research on Fluid Inclusions Conference, Las Vegas, Nevada, June 7-10, 2010.

Lowenstein, T.K., Demicco, R.V., 2006. Elevated Eocene atmospheric CO_2 and its subsequent decline. Science 313, 1928. https://doi.org/10.1126/science.1129555, 1928.

Lowenstein, T.K., Dolginko, L.A.C., García-Veigas, J., 2016. Influence of Magmatic-Hydrothermal Activity on Brine Evolution in Closed Basins: Searles Lake, California, vol. 128. Geological Society of America Bulletin, pp. 1555–1568. https://doi.org/10.1130/B31398.1.

Lowenstein, T.K., Jagniecki, E.A., Carroll, A.R., Smith, M.E., Renaut, R.W., Owen, R.B., 2017. The Green River salt mystery: what was the source of the hyperalkaline lake waters? Earth Sci. Rev. 173, 295–306. https://doi.org/10.1016/j.earscirev.2017.07.014.

Machlus, M.L., Ramezani, J., Bowring, S.A., Hemming, S.R., Tsukui, K., Clyde, W.C., 2015. A strategy for cross-calibrating U–Pb chronology and astrochronology of sedimentary sequences: an example from the Green River Formation, Wyoming, USA. Earth Planet Sci. Lett. 413, 70–78. https://doi.org/10.1016/j.epsl.2014.12.009.

Milton, C., Fahey, J.J., 1960. Classification and association of the carbonate minerals of the Green River Formation. Am. J. Sci. 258, 242–246.

Murphy, J.T., Lowenstein, T.K., Pietras, J.T., 2014. Preservation of primary lake signatures in alkaline earth carbonates of the Eocene Green River Wilkins Peak-Laney Member transition zone. Sediment. Geol. 314, 75–91. https://doi.org/10.1016/j.sedgeo.2014.09.005.

Olson, K.J., Lowenstein, T.K., 2021. Searles Lake evaporite sequences: indicators of late Pleistocene/Holocene lake temperatures, brine evolution, and pCO_2. Geol. Soc. Am. Bull. 133, 2319–2334. https://doi.org/10.1130/B35857.1.

Pietras, J.T., Carroll, A.R., 2006. High-resolution stratigraphy of an underfilled lake basin: Wilkins Peak member, Eocene Green River Formation, Wyoming, USA. J. Sediment. Res. 76, 1197–1214.

Pitzer, K.S., 1991. Ion interaction approach: theory and data correlation. In: Pitzer, K.S. (Ed.), Activity Coefficients in Electrolyte Solutions, vol. 2. CRC Press, Boca Raton, FL, pp. 75–154.

Pretti, V.A., Stewart, B.W., 2002. Solute sources and chemical weathering in the Owens Lake watershed. eastern California: Water Resour. Res. 38, 2. https://doi.org/10.1029/2001WR000370, 1–2-18.

Renaut, R.W., Owen, R.B., Lowenstein, T.K., De Cort, G., McNulty, E., Scott, J.J., Mbuthia, A., 2021. The role of hydrothermal fluids in sedimentation in saline alkaline lakes: evidence from Nasikie Engida, Kenya Rift Valley. Sedimentology 68, 108–134. https://doi.org/10.1111/sed.12778.

Risacher, F., Clement, A., 2001. A computer program for the simulation of evaporation of natural waters to high concentration. Comput. Geosci. 27, 191–201. https://doi.org/10.1016/S0098-3004(00)00100-X.

Smith, M.E., Carroll, A.R., Jicha, B.R., Cassel, E.J., Scott, J.J., 2014. Paleogeographic Record of Eocene Farallon Slab Rollback beneath Western, vol. 42. North America: Geology, pp. 1039–1042. https://doi.org/10.1130/G36025.1.

Smith, M.E., Carroll, A.R., Mueller, E.R., 2008a. Elevated weathering rates in the rocky Mountains during the early Eocene climatic Optimum. Nat. Geosci. 1, 370.

Smith, M.E., Carroll, A.R., Scott, J.J., 2015. Stratigraphic expression of climate, tectonism, and geomorphic forcing in an underfilled lake basin: Wilkins Peak member of the Green River Formation. In: Smith, M.E., Carroll, A.R. (Eds.), Stratigraphy and Paleolimnology of the Green River Formation. Springer Netherlands, Syntheses in Limnogeology, Western USA, Dordrecht, pp. 61–102. https://doi.org/10.1007/978-94-017-9906-5_4.

Smith, M.E., Carroll, A.R., Singer, B.S., 2008b. Synoptic Reconstruction of a Major Ancient Lake System: Eocene Green River Formation, Western United States, vol. 120. Geological Society of America Bulletin, pp. 54–84. https://doi.org/10.1130/B26073.1.

Smith, M.E., Chamberlain, K.R., Singer, B.S., Carroll, A.R., 2010. Eocene clocks agree: Coeval 40Ar/39Ar, U-Pb, and astronomical ages from the Green River Formation. Geology 38, 527–530. https://doi.org/10.1130/G30630.1.

Smith, M.E., Singer, B., Carroll, A., 2003. 40Ar/39Ar Geochronology of the Eocene Green River Formation, Wyoming, vol. 115. Geological Society of America Bulletin, pp. 549–565. https://doi.org/10.1130/0016-7606(2003)115<0549:AGOTEG>2.0.CO;2.

Smoot, J.P., 1983. Depositional subenvironments in an arid closed basin; the Wilkins Peak member of the Green River Formation (Eocene), Wyoming. U.S.A.: Sedimentology 30, 801–827. https://doi.org/10.1111/j.1365-3091.1983.tb00712.x.

Smoot, J., 1978. Origin of the carbonate sediments in the Wilkins Peak member of the lacustrine Green River Formation (Eocene), Wyoming, USA. In: Matter, A., Tucker, M.E. (Eds.), Modern and Ancient Lake Sediments, the International Association of Sedimentologists. Special Publication 2, pp. 109–127. https://doi.org/10.1002/9781444303698.ch6.

Sorey, M.L., 1985. Evolution and present state of the hydrothermal system in Long Valley Caldera. J. Geophys. Res. 90, 11219. https://doi.org/10.1029/JB090iB13p11219.

Tuttle, M.L., Goldhaber, M.B., 1993. Sedimentary sulfur geochemistry of the Paleogene Green River Formation, western USA: implications for interpreting depositional and diagenetic processes in saline alkaline lakes. Geochem. Cosmochim. Acta 57, 3023–3039. https://doi.org/10.1016/0016-7037(93)90291-4.

Wiig, S.V., Grundy, W.D., Dyni, J.R., 1995. Trona resources in the Green River Basin, southwest Wyoming: U.S. Geological survey. Open-File Report USGS Numbered Series 95–476. http://pubs.er.usgs.gov/publication/ofr95476. May 2019.

Wilf, P., 2000. Late Paleocene-early Eocene climate changes in southwestern Wyoming: paleobotanical analysis. Geol. Soc. Am. Bull. 112, 292–307. https://doi.org/10.1130/0016-7606(2000)112<292:LPECCI>2.0.CO;2.

Wolfbauer, C.A., Surdam, R.C., 1974. Origin of Nonmarine Dolomite in Eocene Lake Gosiute, Green River Basin, Wyoming, vol. 85. Geological Society of America Bulletin, pp. 1733–1740. https://doi.org/10.1130/0016-7606(1974)85<1733:OONDIE>2.0.CO;2.

Zachos, J.C., Dickens, G.R., Zeebe, R.E., 2008. An early Cenozoic perspective on greenhouse warming and carbon-cycle dynamics. Nature 451, 279–283.

Zachos, J., Pagani, M., Sloan, L., Thomas, E., Billups, K., 2001. Trends, rhythms, and aberrations in global climate 65 Ma to present. Science 292, 686–693.